

A novel deceleration traffic flow model with oscillatory congested states

Junxia Wang(王君霞) and Tiandong Xu(徐天东)

Citation: Chin. Phys. B, 2025, 34 (**10**): 108902. DOI: 10.1088/1674-1056/add500
http://cpb.iphy.ac.cn; http://iopscience.iop.org/cpb

What follows is a list of articles you may be interested in

Simulation study on cooperation behaviors and crowd dynamics in pedestrian evacuation

Ya-Ping Ma(马亚萍), Hui Zhang(张辉)
Chin. Phys. B, 2020, 29 (**3**): 038901. DOI: 10.1088/1674-1056/ab6b14

A new cellular automaton model accounting for stochasticity in traffic flow induced by heterogeneity in driving behavior

Xiaoyong Ni(倪晓勇), Hong Huang(黄弘)
Chin. Phys. B, 2019, 28 (**9**): 098901. DOI: 10.1088/1674-1056/ab343b

Evacuation flow of pedestrians considering compassion effect

Yu-Zhang Chen(陈煜章), Ming Li(李明), Rui Jiang(姜锐), Mao-Bin Hu(胡茂彬)
Chin. Phys. B, 2018, 27 (**8**): 088901. DOI: 10.1088/1674-1056/27/8/088901

Self-organized phenomena of pedestrian counterflow through a wide bottleneck in a channel

Li-Yun Dong(董力耘), Dong-Kai Lan(蓝冬恺), Xiang Li(李翔)
Chin. Phys. B, 2016, 25 (**9**): 098901. DOI: 10.1088/1674-1056/25/9/098901

Influence of bus stop with left-turn lines between two adjacent signalized intersections

Ming-Bao Pang(庞明宝), Lan-Hang Ye(叶兰杭), Ya-Nan Pei(裴亚男)
Chin. Phys. B, 2016, 25 (**8**): 088901. DOI: 10.1088/1674-1056/25/8/088901

A novel deceleration traffic flow model with oscillatory congested states

Junxia Wang(王君霞)[1,†] and Tiandong Xu(徐天东)[1,2,‡]

[1] *School of Civil Engineering and Transportation, Northeast Forestry University, Harbin* 150040, *China*
[2] *College of Design, Construction, and Planning, University of Florida, Gainesville* 32611, *USA*

(Received 3 March 2025; revised manuscript received 5 May 2025; accepted manuscript online 7 May 2025)

A novel deceleration traffic flow model is established based on the oscillatory congested states and the slow-to-start rule. The novel model considers human overreaction and mechanical restrictions as limited deceleration capacity, effectively avoiding the unrealistic deceleration behavior found in most existing traffic flow models. In order to consider that the acceleration of a stationary vehicle is slower than that of a moving vehicle due to reasons such as driver inattention, the slow-to-start rule is introduced. In actual traffic, the driver will take different deceleration measures according to local traffic conditions, divided into ordinary and emergency deceleration. The deceleration setting in the deceleration model with only ordinary deceleration is modified. Computer simulations show that the novel model can achieve smooth, comfortable acceleration and deceleration behavior. Introducing the slow-to-start rule can realize the first-order transition from free flow to synchronized flow. The oscillatory congested states enable a first-order transition from synchronized flow to wide moving jam. Under periodic boundary conditions, the novel model can reproduce three traffic flow phases (free flow, synchronized flow, and wide moving jam) and two first-order transitions between three phases. In addition, the novel model can reproduce empirical results such as linear synchronized flow and headway distribution of free flow below 1 s. Under open boundary conditions, different congested patterns caused by on-ramps are analyzed. Compared with the classic deceleration model, this model can better reproduce the phenomenon and characteristics of actual traffic flow and provide more accurate decision support for daily traffic management of expressways.

Keywords: oscillatory congested states, three-phase traffic flow, limited deceleration capacity, slow-to-start rule, cellular automaton

PACS: 89.40.–a, 45.70.Vn, 05.65.+b, 05.40.–a

DOI: 10.1088/1674-1056/add500 **CSTR:** 32038.14.CPB.add500

1. Introduction

Traffic congestion causes low traffic efficiency and seriously affects the rapid development of the social economy. The three-phase traffic flow theory has become a research hot spot because it can explain various complex traffic phenomena.[1] The cellular automaton (CA) model has the advantages of good parallelism, flexible evolution rules, and high computational efficiency. It is widely used to clarify the essence of traffic flow dynamics and gradually occupies an essential status in traffic flow theory research. With the advent of the three-phase traffic theory, driver behavior has received considerable attention in cellular automaton modeling, especially oscillations around steady states within the deterministic limit, in order to reproduce empirical phenomena. Therefore, this paper uses the cellular automaton model under the three-phase traffic flow theory framework to establish a novel deceleration traffic flow model based on the oscillatory congested states.

The major drawback of most existing CA models is that all vehicles have no limit to the deceleration capability.[2] Krauss and Wagner[3] first introduced limited deceleration capacity in the CA traffic flow model, but because the value of deceleration capacity is too conservative, the simulation results still have unrealistic deceleration behavior. Lee *et al.*[4] proposed a model considering limited deceleration capability (abbreviated as the Lee model), which is inherently unsafe because a significant deceleration is occasionally required to avoid collisions, so emergency deceleration is introduced in this paper. Based on the Lee model, Pottmeier *et al.*[5] improved the original single-lane model by increasing its robustness to accidents (abbreviated as the Pottmeier model). Vranken *et al.*[6] proposed a single-lane traffic flow model with a time step of 0.1 s, which can simulate the heterogeneous traffic flow with a mixture of human-driven and automated vehicles. Inspired by the idea of deceleration limitation, many scholars have conducted research in this area and achieved fruitful results in the past few decades.[7–11]

It must be emphasized that over-reaction as the reason of the classical traffic flow instability was introduced.[1–8] Chen *et al.*[9] studied traffic hysteresis arising in traffic oscillations from a behavioral perspective. It is found that the occurrence and type of traffic hysteresis is closely correlated with driver behavior when experiencing traffic oscillations and with

†Corresponding author. E-mail: wangjunxia@nefu.edu.cn
‡Corresponding author. E-mail: tdxu@nefu.edu.cn

© 2025 Chinese Physical Society and IOP Publishing Ltd. All rights, including for text and data mining, AI training, and similar technologies, are reserved.

the time driver reaction begins relative to the starting deceleration wave. Outay *et al.*[10] proposed to implement the reaction time-based collaborative velocity control (RT-CVC) model that was implemented in autonomous cars into an agent-based simulator. This model is compared to the intelligent driver model (IDM), which is one of the standard longitudinal driving behaviors in simulation environments. Additionally, there are many papers about microscopic modeling with driver's over-reaction idea.[11–14]

However, the models mentioned above do not consider oscillatory congested states, i.e., in congested traffic flow, the space gap between two vehicles will oscillate around the desired space gap in the deterministic limit.[12] The primary mechanism incorporated into this assumption is in the deceleration of the vehicles. From the perspective of the braking capacity of the vehicles, in addition to ordinary braking in normal conditions, emergency braking is required in emergencies. The model assumes that the vehicles adopt ordinary deceleration in normal conditions and emergency deceleration in emergencies. Guzmán *et al.*[13] proposed a reliable cellular automaton model that faithfully reproduced deceleration and acceleration based on the driver's actual response, considering that vehicles have different deceleration capabilities. The model describes complex traffic phenomena by encoding its rules' fundamental mechanisms of driver behavior, vehicle capabilities, and dynamics. Li *et al.*[14] described the empirical car-following behavior of commercial adaptive cruise control (ACC) systems and understood the behavior of ACC under different conditions. For a three-vehicle platoon, the change from one ACC vehicle to another is progressive for the oscillation growth and decreasing for deceleration, acceleration, and overtaking.

Considering that the acceleration of a stationary vehicle may be slower than that of a moving vehicle due to the driver's inattention and difficulty in starting due to long-term parking, the slow-to-start rule is introduced. Takayasu and Takayasu[15] first proposed the CA model with a slow-to-start rule (abbreviated as the TT model). Schadschneider *et al.*[16] proposed an extended model based on the TT model. The model further specifies the acceleration behavior, and the update rule is: if there is precisely an empty cell in front of the stationary vehicle in the system, the vehicle will accelerate with a probability of 0.25; for other cases, it still accelerates according to the deterministic rules of the Nagel and Schreckenberg (NaSch) model.[17] Barlovic *et al.*[18] proposed velocity-dependent-randomization (VDR) model. The difference between the VDR model and the NaSch model is that the randomization probability is no longer fixed but determined by the vehicle's velocity at the last moment, and the rest of the update rules are the same as the NaSch model. Gao *et al.*[19] proposed a cellular automaton model with velocity adaptation, equivalent to combining the Kerner–Klenov–Wolf (KKW) model[20] and the NaSch model with a slow-to-start rule. Qiao *et al.*[21] studied phase diagrams to reflect traffic congestion and PM emissions for two typical slow-to-start models under open boundary conditions. Importantly, with the introduction of the slow-to-start rule, it can be found that the flow drop occurs near the phase transition point from synchronized flow to wide moving jam.[22,23]

This paper aims to describe driver behavior and vehicle braking capability through a novel deceleration traffic flow model that considers oscillatory congested states and slow-to-start rules, reproducing some empirical results of the three-phase traffic flow theory. The rest of this paper is structured as follows. The first section reviews Kerner's three-phase traffic flow theory. Section 2 details the model rules. Simulation results under periodic boundary conditions are simulated and discussed in Section 3. Simulation results with open boundary conditions are simulated and discussed in Section 4. Section 5 gives a summary.

2. Review of Kerner's three-phase traffic flow theory

Nagel and Schrekenberg[17] first proposed a classic cellular automaton model (the NaSch model) consisting of four parallel update rules. The traffic flow is divided into free flow and congested flow in the two-phase models.[2,3,16,18]

By analyzing field data, Kerner proposed the famous three-phase traffic flow theory and divided the congested flow into the synchronized flow (S) and wide moving jam (J).[1–4,24–26] The synchronized flow is defined as its downstream front at the highway bottleneck and ensures the nucleation nature of traffic breakdown (F→S transition). A wide moving jam is a moving jam that maintains the average velocity of the downstream front of the jam as it propagates, even as it propagates through bottlenecks or other diverse, complex traffic states.[13,27]

Commonly observed traffic phase transitions from large empirical datasets are the phase transition from free flow to synchronized flow (F→S transition) and the phase transition from synchronized flow to wide moving jam (S→J transition). The F→S transition and the S→J transition are first-order transitions, during which the flow rate drops sharply. Two-step F→S→J transition: the F→S transition occurs first, and then the S→J transition occurs at different positions after a while, where the F→S→J transition shows double Z characteristic in the velocity-density plane, while the line J becomes a curve in the flow-density plane. Related to this phenomenon, two main types of congested patterns at isolated bottlenecks can be observed.

General patterns (GPs) and synchronized flow patterns (SPs).[28] GPs consist of free flow, synchronized flow, and

wide-moving jam. When the traffic flow is in the SPs, there are free flow and synchronized flow on the road. As a result of the bottleneck, various types of SPs may occur, such as widening synchronized pattern (WSP), local synchronized pattern (LSP), and moving synchronized pattern (MSP).

Kerner and Klenov proposed the first cellular automaton model for three-phase traffic flow.[29] The same year, Kerner *et al.* proposed a microscopic model to reproduce the typical characteristics of three-phase traffic flow, abbreviated as the KKW model.[20] Kerner *et al.*[30] established a novel three-phase CA traffic flow model based on the discontinuous characteristics of drivers' excessive acceleration. Based on the KKW model, Zeng *et al.*[31] proposed a traffic flow model of the freeway ramp system under accident conditions and simulated and analyzed the impact of traffic accidents on traffic flow under open boundary conditions. Based on the Kerner–Klenov–Schrecenberg–Wolf (KKSW) cellular automaton model,[32] Hu *et al.*[33,34] established a two-way six-lane expressway model. They studied the impact of tidal lanes and entry points on urban traffic flow in the framework of Kerner's three-phase traffic theory and achieved good results. Lyu *et al.*,[35] based on the improved KKSW cellular automaton model, studied the vehicle–vehicle non-uniform traffic flow characteristics of the expressway with climbing lanes. Zhao *et al.*[27] established a modified velocity difference effect (MVDE) model based on Kerner's three-phase traffic flow theory. Under the three-phase traffic theory framework, the MVDE model showed better-synchronized flow results. Zhou *et al.*[36] proposed the multi-anticipative model (MAM) based on the average space gap model, describing the impact of multi-anticipatory effects on acceleration and deceleration. Simulations show that MAM can reproduce empirically consistent synchronized flow and associated congested patterns well.

3. Model formulation

Considering the oscillatory congested states, the novel model introduces an effective desired space gap $d_n^*(t)$ in the update rule. Assuming that the driver tends to keep the effective space gap not smaller than $d_n^*(t)$, otherwise, the driver will be in a defensive state, and the actual behavioral change is characterized by changing deceleration from 1 $L_{\text{cell}}/\text{s}^2$ to 4 $L_{\text{cell}}/\text{s}^2$. The effect of deceleration changing from ordinary deceleration to emergency deceleration is a critical factor in reproducing the phase transition from free flow to synchronized flow in the novel model. The following formula determines the determination of deceleration:

$$D=\begin{cases}4, & \text{if } d_n^{\text{eff}}(t)<d_n^*(t),\\ 1, & \text{else},\end{cases} \tag{1}$$

$$d_n^*(t)=Tv_n(t), \tag{2}$$

$$d_n^{\text{eff}}(t)=d_n(t)+\max(v_{\text{anti}}(t)-g_{\text{safety}},0), \tag{3}$$

$$v_{\text{anti}}(t)=\min(d_{n+1}(t),v_{n+1}(t)+1,v_{\max}). \tag{4}$$

Here, $d_n(t)$ is the space gap between vehicle n and its previous vehicle $n+1$, $d_n^*(t)$ is the effective desired space gap between vehicles n and $n+1$, and $d_n^{\text{eff}}(t)$ is the effective space gap. T is the effective safe time gap between vehicles n and $n+1$ in steady state, and $v_{\text{anti}}(t)$ is the expected velocity of the vehicle ahead at the next time step. g_{safety} is the parameter controlling the validity of the anticipation.

In the novel model, the velocity to ensure safe driving is denoted by c_n^{t+1}, which should satisfy the following inequality:

$$\begin{aligned}&x_n^t+\Delta+\sum_{i=0}^{\tau_{\text{f}}(c_n^{t+1})}(c_n^{t+1}-Di)\\ &\le x_{n+1}^t+\sum_{i=1}^{\tau_{\text{l}}(v_{n+1}^t)}(v_{n+1}^t-Di).\end{aligned} \tag{5}$$

Among them c_n^{t+1}: safe velocity of vehicle n at time $t+1$. x_n^t, v_n^t: the position (velocity) of the follower vehicle at time t. n ($n+1$): the follower vehicle (the leader vehicle). D: deceleration. τ_{f} (τ_{l}): the time step required for the follower vehicle (the vehicle in front) to decelerate continuously to a complete stop. The summation starting from zero represents the response time of the follower vehicle, so for the follower vehicle, the cumulative sum is calculated from the time step $i=0, 1, \ldots, \tau_{\text{f}}$, and for the leader vehicle, it is calculated from time step $i=1, 2, \ldots, \tau_{\text{l}}$. Δ: the minimum coordinate difference required by the follower vehicle to ensure safety must be at least the length of one vehicle. The expressions τ_{f}, τ_{l}, and Δ are detailed later to account for human overreactions.

$$\tau_{\text{f}}(v)=\gamma_n^t v/D+(1-\gamma_n^t)\max\{0,\min\{v/D,t_{\text{safe}}\}-1\}, \tag{6}$$

$$\tau_{\text{l}}(v)=\gamma_n^t v/D+(1-\gamma_n^t)\min\{v/D,t_{\text{safe}}\}, \tag{7}$$

$$\Delta=L+\gamma_n^t\max\{0,\min\{g_{\text{add}},v_n^t-g_{\text{add}}\}\}. \tag{8}$$

Here t_{safe} means the maximum time step that the follower vehicle can predict its safety when driving optimistically, but g_{add} is the additional safe time gap required when driving pessimistically. The additional -1 for the follower vehicle is the reaction time that is only compensated for driving optimistically, and the function of t_{safe} is implemented at the same time. A two-state variable is introduced to reflect the driver's discriminatory behavior towards local traffic conditions. When $\gamma_n^t=0$, it corresponds to the situation where the driver judges the local situation as optimistic because the vehicle in front is accelerating. Conversely, when $\gamma_n^t=1$, the driver is pessimistic, and the vehicle needs to decelerate below the velocity required by the strict no-collision standard. γ_n^t is defined as follows:

$$\gamma_n^t=\begin{cases}0, & \text{for } v_n^t\le v_{n+1}^t<v_{n+2}^t \text{ or}\\ & (v_{n+2}^t\ge v_{\text{fast}}\bigwedge v_n^t-v_{n+1}^t\le D\bigwedge b_{n+2}^t=0),\\ 1, & \text{otherwise.}\end{cases} \tag{9}$$

The faster velocity v_{fast} slightly below maximum velocity $v_{\max}$, and both variables are assumed to be constant. In addition, for variable γ_n^t, considering that each vehicle n and vehicle $n+2$ require a stronger interaction in order to prevent the occurrence of two situations that may lead to dangerous configurations in the Lee model, the relationship between v_{n+1} and v_{n+2} is strengthened in the novel model to satisfy the condition $v_{n+1} < v_{n+2}$, and use the maximum braking capacity to limit the difference between v_n and v_{n+1}. It indicates whether the vehicle decelerates due to the surrounding environment rather than randomness. The brake light b_n^t is defined as follows:

$$b_n^t = \begin{cases} 1, & \text{for } \tilde{v}_n^{t+1} < v_n^t, \\ 0, & \text{otherwise.} \end{cases} \tag{10}$$

Here b_n^t: the states of the brake light of vehicle n at time t and $b_n^t = 1$ (0) means the brake light is on (off). $\tilde{v}_n^{t+1}$: the saved velocity before randomization. To sum up, for $\gamma_n^t = 0$, τ_{f}, τ_{l} will be smaller than v/D, and Δ is close to vehicle length L. At this time, the safety condition is loose, and a faster $\tilde{c}_n^{t+1}$ can be selected; on the other hand, for $\gamma_n^t = 1$, τ_{f}, τ_{l} are close to v/D, Δ will be greater than vehicle's length L, and the safety condition is more necessary, a slower $\tilde{c}_n^{t+1}$ can be specified. The parallel update rules for the novel model consist of the following five steps.

Step 1 Determination of the randomization probability p

$$p = \max\{p_{\text{d}},\ p_0 - v_n^t(p_0 - p_{\text{d}})/v_{\text{slow}}\}. \tag{11}$$

Step 2 Determination of the maximal safe velocity

$$\tilde{c}_n^{t+1} = \max\{c_n^{t+1} | c_n^{t+1} \text{ satisfies Eqs. (1)–(10)}\}. \tag{12}$$

Step 3 Acceleration and deceleration

If $v_n^t = 0$ and gap $= 1$, vehicles will stay in their original position and not move with probability $p_t = 0.75$, else

$$\tilde{v}_n^{t+1} = \min\{v_{\max}, v_n^t + a, \max\{0, v_n^t - D, \tilde{c}_n^{t+1}\}\}. \tag{13}$$

Step 4 Randomization with probability p

$$v_n^{t+1} = \max\{0, v_n^t - D, \tilde{v}_n^{t+1} - \eta\}, \tag{14}$$

$$\eta = \begin{cases} 1, & \text{if rand}(\,) < p, \\ 0, & \text{else.} \end{cases} \tag{15}$$

Step 5 Vehicle movement

$$x_n^{t+1} = x_n^t + v_n^{t+1}. \tag{16}$$

In the update rules, the third step introduced the slow-to-start rules of the Takayasu and Takayasu model[15] and modified them. A stationary vehicle with only one empty cell in front stops in the same place with the probability of p_t; otherwise, the acceleration and deceleration are updated according to the formula (13). The randomization probability p in Step 1 is linearly interpolated between p_0 and p_{d} when it is less than v_{slow}, and p_{d} is adopted for p when v_n^t is greater than v_{slow}. In addition, p is an actual number, and the novel model assumes that $p_0 > p_{\text{d}}$. It should be emphasized that for a given vehicle n, the safe velocity can take on the value of about $0 - v_{\max}\ L_{\text{cell}}/\text{s}$ at most, and it has multiple values in most cases. In order to reflect the desire of the driver to drive as fast as possible, the maximum safe velocity is taken and expressed by $\tilde{c}_n^{t+1}$. The gap is the number of empty cells in front of the vehicle n. It is important to note that both Step 3 and Step 4 involve limited deceleration capacity. The position update is conducted at last.

4. Simulation investigation

4.1. Simulation results under the periodic boundary condition

The general characteristics of the novel model are studied on the ring road. The unit time step corresponds to 1 s. All key parameters and its definitions are listed in Table 1, which are different from the Lee model to be more in line with the actual situation. The simulation is carried out on the road of $L_{\text{road}} = 4 \times 10^4\ L_{\text{cell}}$ length. Stationary vehicles are initially evenly distributed on the road to avoid the impact of uneven distribution of the initial vehicle on the simulation results. During the simulation, the first 4.9×10^5 s is conducted to make the transient disappear, the system reaches steady state, and the simulation time step is set to 5×10^5 s, so the statistics are collected in the last 1×10^4 s. On the premise of ensuring the reliability of statistical results, considering the limitations of computing resources, the number of samples in this article is 50.

Table 1. Definition and value of parameters in the novel model.

Parameters	Value	Units	Definition
L_{cell}	1.5	m	length of each cell
L_{veh}	5	L_{cell}	vehicle length
$v_{\max}$	20	L_{cell}/s	maximum velocity
v_{fast}	19	L_{cell}/s	faster velocity
v_{slow}	5	L_{cell}/s	slower velocity
p_0	0.32	–	randomization probability
p_{d}	0.11	–	randomization probability
p_t	0.75	–	randomization probability
a	1	$L_{\text{cell}}/\text{s}^2$	acceleration
t_{safe}	3	s	maximum time step
g_{add}	4	L_{cell}	additional safe time gap

Figures 1(a) and 1(b) draw a dotted line on the flow–density and velocity–density planes, in which three traffic flow phases (free flow, synchronized flow, and wide moving jam) and two first-order phase transitions between the three phases (from free flow to synchronized flow (F→S transition) and from synchronized flow to wide moving jam (S→J transition) are distinguished. The straight line with a positive slope of the

red sphere represents free flow, the negative slope of the blue sphere represents synchronized flow, and the longest line with a negative slope of the green sphere represents a wide moving jam. When the density K is less than K_1, only the free flow can be found in the diagram (Fig. 2(a)). With the increase of density, the flow increases until $K = K_1$, and the maximum flow is close to 2250 veh/h. When the density is more significant than K_1, the synchronized flow forms spontaneously from the free flow, as shown in Figs. 2(b) and 1(c). With further density increase, the range of synchronized flow expands, and the velocity decreases (Fig. 2(c)). When the density is more remarkable than K_2, the synchronized flow is unstable, and a wide-moving jam occurs (Fig. 2(d)). Figure 2(d) shows the vehicle's trajectory as it approaches the upstream front of the traffic jam, which reveals that the revised update rules modify the unrealistic sudden velocity drop. Similarly, vehicles can accelerate smoothly and comfortably when they leave the downstream of the traffic jam. The flow decreases significantly when the density returns to K_3, as shown in Fig. 1(d). In addition, when $K > K_3$, the wide moving jam with lower velocity appears. It can be found that the downstream propagation speed of the wide moving jam is nearly -15 km/h, which is consistent with the empirical observation. This indicates that the new model can reproduce the same propagation characteristics of the congestion pattern that are consistent with the three-phase traffic theory. For a more explicit description, the flux, velocity, and density are converted into vehicles per hour, kilometer per hour, and vehicles per kilometer, respectively.

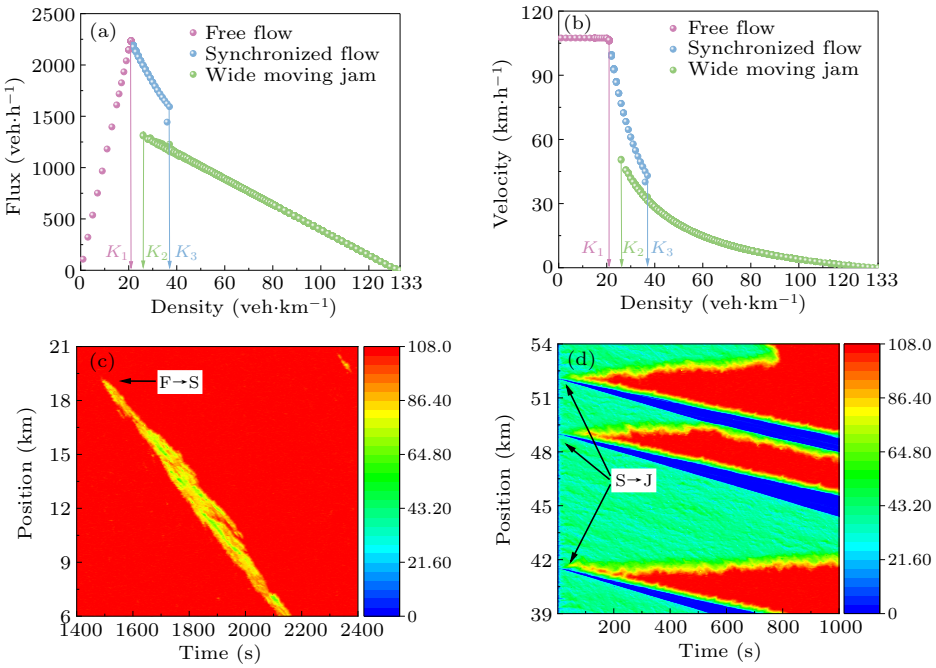


Fig. 1. The fundamental diagram and the spatiotemporal diagrams: (a) the fundamental diagram (FD) on the flux–density plane, (b) the fundamental diagram on the velocity–density plane, (c) $K = 21$ veh/km, describes the F→S transition and (d) $K = 37$ veh/km, describes the S→J transition. The color bar indicates velocity (km/h).

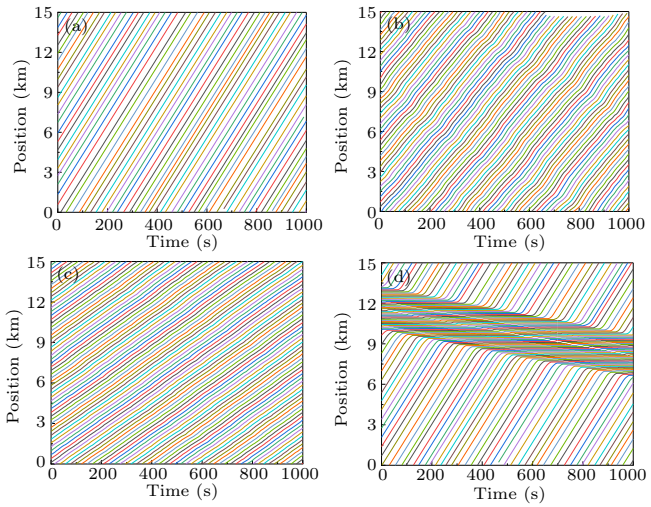


Fig. 2. Trajectories of every 10th vehicle of the novel model, where (a) $K = 15$ veh/km, (b) $K = 25$ veh/km, (c) $K = 35$ veh/km, (d) $K = 40$ veh/km, respectively.

Figures 3(a) and 3(b) show the one-minute averaged flow and density in new model and the pottmeier model, in which the maximum flow and its corresponding density are almost consistent with the empirical data. A virtual detector at the road's midpoint monitors the flow (J) and velocity (V) arithmetic average. The local density (ρ) on the x-axis is calculated by $\rho = J/V$. In addition, the straight line with a positive slope corresponds to the free flow, and the synchronized flow is widely dispersed in the two-dimensional (2D) area of the diagram. The synchronized flow generally shows a linear distribution in new model, however, linear synchronized flow is not observed in the Pottmeier model, which is consistent with the fundamental diagram representation. The flow of the synchronized flow decreases with the increase of the global density K.

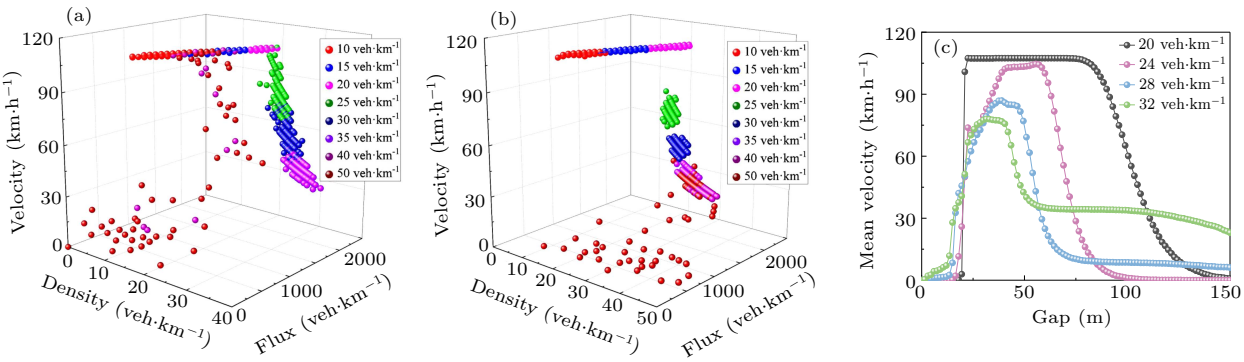


Fig. 3. (a) The one-minute averaged flux and local density in new model, (b) the one-minute averaged flux and local density in pottmeier model, and (c) optimal velocity function.

The novel model makes an in-depth study from the point of view of the headway distribution. Figure 4 shows the headway distribution of different phases (the detector is located at the road's midpoint), which shows the relative frequency of the headway between two adjacent vehicles passing through the detector. The distribution is standardized, and the minimum interval of the headway is 0.2 s. The data is classified by density value. Specifically, under the density corresponding to the free flow, it is mainly distributed in 1 s–3 s, and the position of the maximum value is independent of the density and is fixed at 1.5 s, as shown in Fig. 4(a). However, within the density corresponding to the synchronized flow, the position of the maximum value depends on the density, as shown in Fig. 4(b). With the increase in density, the position of the maximum distribution increases gradually. Under the density of synchronized flow, the headway is more concentrated, which is about 2 s. In addition, the headway approximately obeys the normal distribution. As shown in Fig. 4(c), compared with the phase of the synchronized flow, the ratio of the headway of wide moving jam is more uniform; the distribution is mainly concentrated in 1 s–5 s. Because vehicles with a headway greater than 4 s will not follow other vehicles, vehicles with a headway greater than 4 s account for a relatively low proportion in the model.[37]

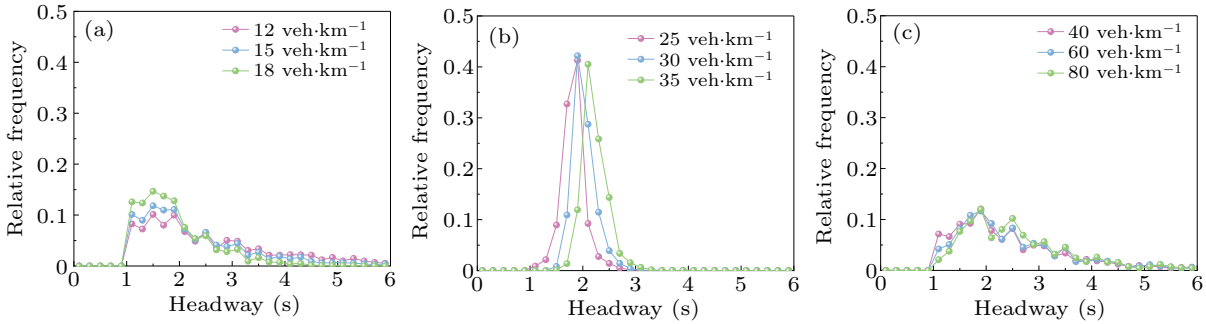


Fig. 4. Normalized headway distributions of the novel model in (a) free flow, (b) synchronized flow, and (c) wide moving jam are depicted for different densities, respectively.

Figure 5 shows the distribution of vehicle velocity at different densities. In free flow, the vehicle's velocity is always close to vmax due to the randomization effect, as shown in Fig. 5(a). As shown in Fig. 5(b), the synchronized flow spontaneously forms from the free flow. As the density increases, the velocity of the synchronized flow decreases, as shown in Fig. 5(c). Figure 5(d) shows wide-moving jams in the synchronized flow. In addition, the velocity of the synchronized flow obeys the normal distribution, which is in good agreement with the actual traffic conditions.

The time series corresponding to the one-minute averaged velocity and flow under the density K_3 is shown in Fig. 6. Different random seeds may show different phases. Figures 6(a) and 6(c) correspond to the synchronized flow of the upper branch at the density K_3 of Fig. 1(a), while figures 6(b) and 6(d) correspond to the wide-moving jam of the lower branch at the density K_3 of Fig. 1(a). One can see that the velocity interruption occurs in about 8200 minutes, accompanied by the flow interruption. Because no vehicle passes through the virtual detector during the interruption, the wide-moving jam's velocity is zero, significantly different from the non-zero velocity in the synchronized flow.

The optimal velocity (OV) function point diagrams of free flow and synchronized flow are primarily separate, as shown in Fig. 3(c). In the free flow region, the averaged velocity is limited by the maximum velocity and is independent of the global density.[38] In the phase of synchronized flow, the averaged velocity of a given gap is much lower than that in the free flow, which means that the vehicle moves much slower than the gap allows to ensure safety. The gap shortens with

the increase in density, and the corresponding averaged velocity decreases. In the case of a large gap, the OV function curve of the synchronized flow region with high density is an approximately normal distribution. The OV function of the model is the direct influence of the vehicle–vehicle interaction, which is consistent with the experimental results.

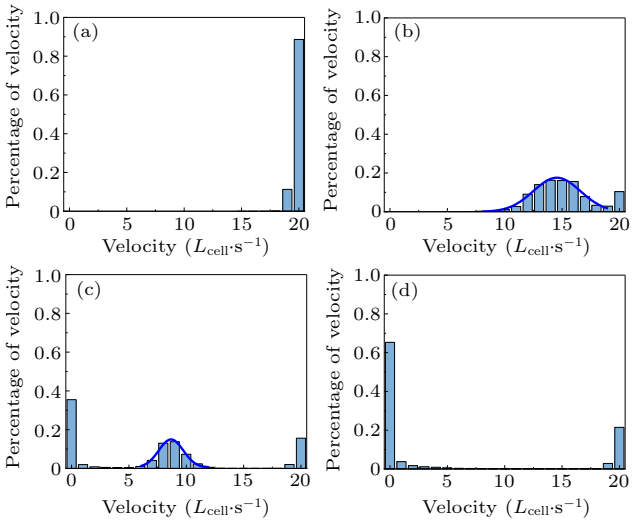


Fig. 5. Histograms of the statistical distribution of velocity, where (a) $K =$ 15 veh/km, (b) $K = 25$ veh/km, (c) $K = 35$ veh/km, and (d) $K = 40$ veh/km.

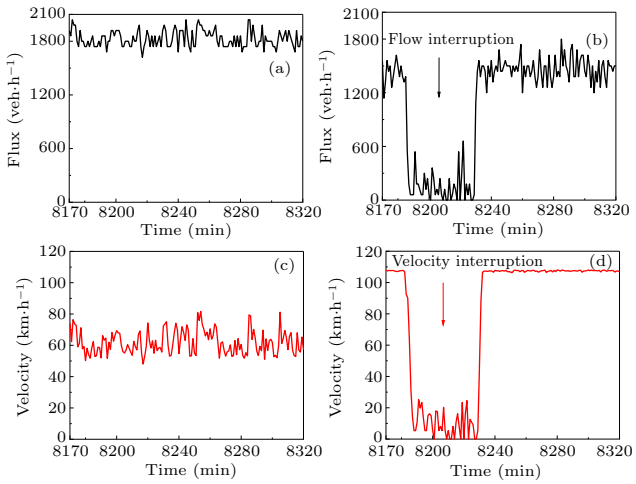


Fig. 6. Time series of one-minute averaged velocity and flow.

The moderate emergency deceleration in the process of vehicle driving can not only ensure the safety of the vehicle but also improve the capacity of the road. Excessive emergency deceleration may waste capacity. In this paper, emergency deceleration is the critical parameter. In order to further analyze the influence of this parameter on traffic flow, a sensitivity analysis is carried out. In the sensitivity analysis, the values of emergency deceleration are set to 2 $L_{\text{cell}}/\text{s}^2$, 3 $L_{\text{cell}}/\text{s}^2$, 4 $L_{\text{cell}}/\text{s}^2$, and 5 $L_{\text{cell}}/\text{s}^2$, respectively. The results of the sensitivity analysis are shown in Fig. 7(a). When the emergency deceleration changes gradually from 2 $L_{\text{cell}}/\text{s}^2$ to 4 $L_{\text{cell}}/\text{s}^2$, the transitions, including F→S transition and S→J transition, still exist, so that the F→S transition can be easily found under the emergency deceleration of 4 $L_{\text{cell}}/\text{s}^2$. In addition, the flow is gradually increasing. With the increase of emergency deceleration, the density region of synchronized flow is shortened, and the density region of wide moving jam is widened. More importantly, the linear synchronized flow becomes the scatter synchronized flow (the synchronized flow is distributed in the two-dimensional region in the middle of the flow-density plane). When the emergency deceleration increases to 5 $L_{\text{cell}}/\text{s}^2$, the synchronized flow does not occur spontaneously, and the transitions no longer exist. Therefore, when the emergency deceleration is 4 $L_{\text{cell}}/\text{s}^2$, the traffic flow is easier to reach a steady state.

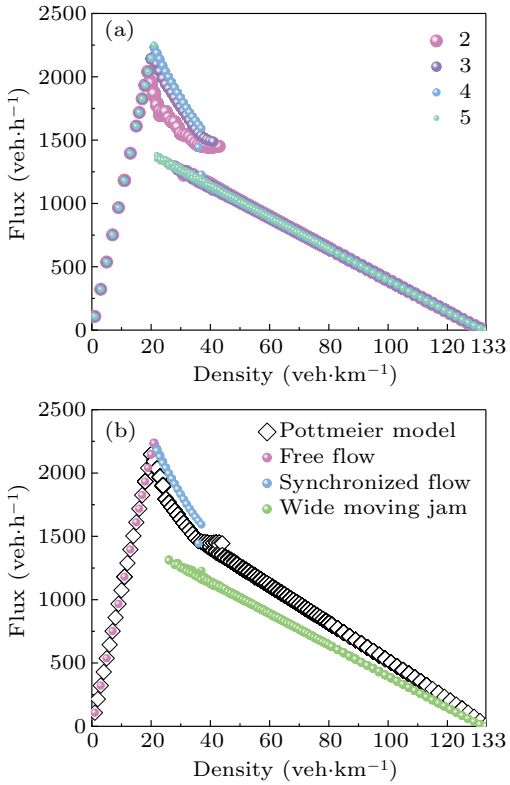


Fig. 7. The fundamental diagrams for comparing: (a) sensitivity analysis of vehicle's emergency deceleration and (b) fundamental diagram of the traditional model and the novel model.

A comparison of the level of improvement achieved with the novel model and the traditional model is presented in Fig. 7(b). The black hollow represents the Pottmeier model, and the color sphere represents the novel model. Compared to the Pottmeier model, oscillatory congested states and the slow-to-start rule are considered in the novel model. The novel model can reasonably simulate the first-order transition from free flow to synchronized flow and from synchronized flow to wide moving jam. At the same time, the linear synchronized flow can be simulated.

Figure 8 presents the FD of the new model in different system sizes. Based on the simulation results, one notes that the transitions including F→S transition and S→J transition always exist as the size of the system increases. Moreover, it should be pointed out that the linear synchronized flow still ex-

ists as the size of the system decreases. It can be clearly found that the density range corresponding to the synchronized flow and wide moving jams is different due to the different system sizes.

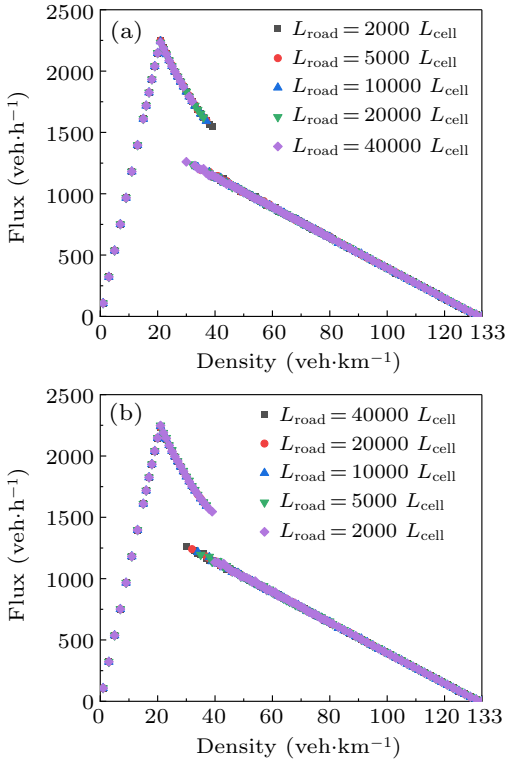


Fig. 8. Fundamental diagram of the new model in different system sizes. (a) Road length decreases from large to small. (b) Road length increases from small to large.

4.2. Simulation results under the open boundary condition

We have simulated an open road consisting of a total length $1.8 \times 10^5\ L_{cell}$ (90 km), whose coordinates are -45 km to 45 km from left to right, and drivers also drive from left to right. The open road has an on-ramp length of $L_{ramp} = 0.6$ km and is at $X_{ramp} = 20.4$ km. The on-ramp starts at the location of X_{ramp} and ends at the location of $X_{ramp} + L_{ramp}$. During simulations, a flow enters the main road constantly from the left of the road. When vehicles enter the main road keeping for 10 hours, the simulation time step is set to zero, and the on-ramp injection Q_{on} is started after 8 min. The number of samples is set to 1.

The model sets the left-most cell of the main road corresponding to the position $x = 1$. Q_{in} and Q_{on} are the traffic flow of the main road and the on-ramp, respectively, in-vehicle units per hour. At each time step, at the entrance of the main road, if the position of the left-most vehicle $X_{last} > v_{max}$, a new vehicle with velocity v_{max} will be injected at the position min $[X_{last} - v_{max}, v_{max}]$ with a probability of $Q_{in}/3600$, where $[\,]$ is the rounding function. If the leading vehicle's position is $X_{lead} > L_{road}$ at the main road's exit, the leading vehicle will be removed, and the following vehicle becomes the leader.

In addition, the condition of whether an entering vehicle injects into the main road from the on-ramp or not plays an important role. Within the merging road section $[X_{ramp}, X_{ramp} + L_{ramp}]$, two consecutive vehicles with the widest gap are selected, and X_l and X_f denote their coordinates. The entering vehicle will be placed at the coordinate $X_{enter} = \lfloor X_f + L_{veh} + (X_l - X_f - 2L_{veh})/2 \rfloor$ (where $\lfloor X \rfloor$ denotes the most significant integer smaller than X) with probability $Q_{on}/3600$ if the widest gap $(X_l - X_f - 2L_{veh})$ between the two consecutive vehicles on the main road exceeds the critical value $d_{critical}$ $(= 0.5V_l + 2L_{veh})$, where V_l is the velocity of leader vehicle of the entering vehicle. The widest gap subtracts the length of the new entering vehicle simultaneously for simplicity. In order to generate a sufficient velocity perturbation in the merging region, the velocity of the entering vehicle is set as 0.7 times that of the respective following vehicle. The stop time is set to zero to keep matters simple.

When traffic breakdown happens near the on-ramp, various congested patterns can occur. Figures 9(a) and 9(b) show the spatiotemporal diagrams of two well-known patterns under open boundary conditions with an on-ramp, including a localized synchronized pattern (LSP, Fig. 9(a)) and a general pattern (GP, Fig. 9(b)). In Fig. 9(a), the downstream front of the synchronized flow is fixed at the on-ramp. The upstream front of the synchronized flow is not continuously widening over time but is localized within 4 km near the bottleneck. Thus, it belongs to the local synchronized pattern (LSP). Figure 9(b) shows the spatial–temporal features of the general pattern (GP). It can be seen that the wide-moving jam continuously emerges in sequence in GP.

In the GP pattern, the synchronized flow appears upstream of the merging region, and wide moving jams spontaneously emerge in the synchronized flow. The downstream fronts of the jams move upstream with a constant speed and widen continuously. This process is indicated in Figs. 9(c) and 9(d), showing the one-minute average flow (c) and velocity (d) at different locations over time in the GP. From the top, virtual detectors are located at 20.4 km, 18.9 km, 15.9 km, and 5.4 km, respectively. The top figure is formed at the beginning of the on-ramp. At the top, it can be seen that a synchronized flow (high flow and low velocity) formed near the on-ramp. In the subsequent two figures, many small flow drops converge upstream into little jams. Finally, some wide jam appeared upstream immediately, away from the on-ramp. It shows the so-called pinch effect,[39] describing the process of local self-organization within the synchronized region, leading to the formation of a small narrow jam. As the minor jams grow large enough to lose the stability of the synchronized flow, these minor jams eventually evolve into several wide-moving jams by merging when moving upstream.

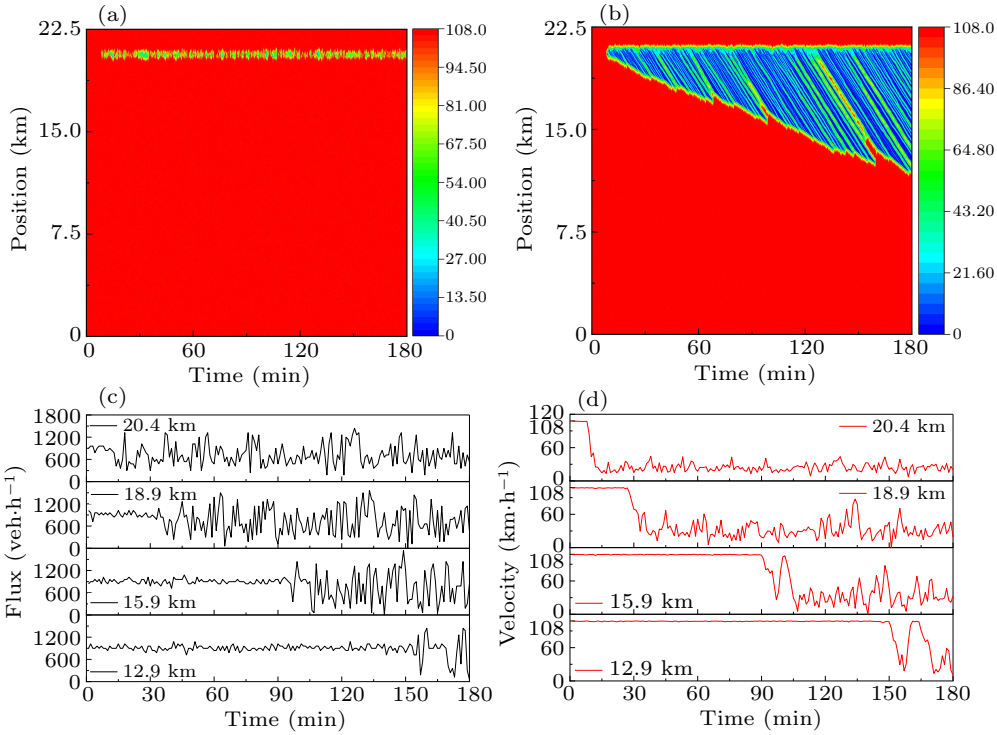


Fig. 9. The spatiotemporal diagrams on open roads with on-ramps: (a) LSP, $(Q_{\text{in}},\ Q_{\text{on}}) = (1700, 400)$ veh/h; (b) GP, $(Q_{\text{in}}, Q_{\text{on}}) = (2100, 900)$ veh/h; (c) and (d) the pinch effect in panel (b).

5. Conclusions

Under the three-phase traffic flow theory framework, introducing the slow-to-start rule proposes a novel deceleration traffic flow model considering oscillatory congested states. Concerning oscillatory congested states, drivers take different deceleration measures according to local traffic conditions, divided into ordinary deceleration (1 $L_{\text{cell}}/\text{s}^2$) and emergency deceleration (4 $L_{\text{cell}}/\text{s}^2$). The deceleration setting of only ordinary deceleration in the deceleration model is modified. The novel model adopts the definition of driver behavior proposed by Pottmeier *et al*. and considers human overreaction and mechanical limitation in the form of limited deceleration capacity, which effectively avoids the unrealistic deceleration behavior found in most of the existing traffic flow models and realizes smooth and comfortable acceleration and deceleration behavior. The slow-to-start rule is introduced into the deceleration model, which considers that the acceleration of the stationary vehicle is more limited than that of the moving vehicle because of the driver's inattention or the need to expend a large amount of traction when starting.

Considering the oscillatory congested states, the model can reasonably simulate the first-order transition from free flow to synchronized flow, and by introducing the slow-to-start rule, the model can reasonably simulate the first-order transition from synchronized flow to wide moving jam. The simulation is carried out under periodic and open boundary conditions, respectively. The results show that the model can better modify the unrealistic deceleration behavior to reflect the driver's behavior in the actual traffic.

The simulation results under periodic boundary conditions show that the novel model can effectively reproduce the three phases of traffic flow (free flow, synchronized flow, and wide moving jam) and the first-order phase transition between them (F→S transition and S→J transition). The model can reproduce the small headway of less than 1s in the free flow phase. The synchronized flow is linear, with only one slope. What is essential is that the reappearance of linear synchronized flow is verified by the trajectory figures, headway distribution figures, velocity distribution histograms, optimal velocity function figures, and so on. The virtual detector finds the velocity interruption accompanied by flow interruption for wide moving jams.

Simulations on open roads with on-ramp show that the novel model can describe the LSP and GP. Both the upstream and downstream of LSP fluctuate near the on-ramp. In the GP, the synchronized flow appears upstream of the merging area, and the wide-moving jams occur spontaneously.

In future research, given the heterogeneity of the application scene, we will further design a two-lane heterogeneous traffic flow model of cars and trucks to discuss the traffic flow characteristics in depth.

Acknowledgements

Project supported by the National Natural Science Foundation of China (Grant No. 71671109), the National Key Research and Development Program of China (Grant No. 2020YFB1600500), and the Key Research and Devel-

opment Program of Heilongjiang Province, China (Grant No. GZ20220089).

References

[1] Tian J F, Zhu C Q, Jiang R and Treiber M 2020 *Transportmetrica A: Transport Science* **2020** 1
[2] Maerivoet S and Moor B D 2005 *Phys. Rep.* **419** 1
[3] Krauss S, Wagner P and Gawron C 1997 *Phys. Rev. E* **55** 5597
[4] Lee H K, Barlovic R, Schreckenberg M and Kim D 2004 *Phys. Rev. Lett.* **92** 238702
[5] Pottmeier A, Thiemann C, Schadschneider A and Schreckenberg M 2007 *Traffic and Granular Flow'*05. Springer, Berlin, Heidelberg, p. 503
[6] Vranken T, Sliwa B, Wietfeld C and Schreckenberg M 2021 *Physica A* **570** 125792
[7] Lan L W, Chiou Y C, Lin Z S and Hsu C C 2009 *Physica A* **388** 3917
[8] Kokubo S, Tanimoto J and Hagishima A 2011 *Physica A* **390** 561
[9] Jin C J, Wang W, Gao K and Jiang R 2011 *Chin. Phys. B* **20** 064501
[10] Shang H Y and Peng Y 2012 *J. Stat. Mech.* **2012** P10001
[11] Lee H K, Kim J, Kim Y and Lee C K 2015 *J. Stat. Mech.* **2015** P06019
[12] Tian J F, Treiber M, Ma S F, Jia B and Zhang W Y 2015 *Transp. Res. B Method.* **71** 138
[13] Guzmán H A, Lárraga M E, Alvarez-Icaza L and Carvajal J 2018 *Physica A* **491** 528
[14] Li T N, Chen D J, Zhou H, Laval J and Xie Y C 2021 *Transp. Res. B Method.* **147** 67
[15] Takayasu M and Takayasu H 1993 *Fractals* **1** 860
[16] Schadschneider A and Schreckenberg M 1997 *Ann. Phys.* **509** 541
[17] Nagel K and Schreckenberg M 1992 *J. Phys. I* **2** 2221
[18] Barlovic R, Santen L, Schadschneider A and Schreckenberg M 1998 *Eur. Phys. J. B* **5** 793
[19] Gao K, Jiang R, Hu S X, Wang B H and Wu Q S 2007 *Phys. Rev. E* **76** 026105
[20] Kerner B S, Klenov S L and Wolf D E 2002 *J. Phys. A: Math. Gen.* **35** 9971
[21] Qiao Y F, Xue Y, Wang X, Cen B L, Wang Y, Pan W and Zhang Y X 2021 *Physica A* **574** 125996
[22] Fu D J, Li Q L, Jiang R and Wang B H 2020 *Physica A* **559** 125075
[23] Li Q L, Wang J X, Ye L L, Jiang R and Wang B H 2023 *Int. J. Mod. Phys. C* **34** 2350120
[24] Kerner B S 1998 *Phys. Rev. Lett.* **81** 3797
[25] Kerner B S, Rehborn H, Aleksic M and Haug A 2004 *Transp. Res. C Emerg. Technol.* **12** 369
[26] Kerner B S and Klenov S L 2009 *Transp. Res. Rec.* **2124** 67
[27] Zhao H T, Lin L, Xu C P, Li Z X and Zhao X 2020 *Physica A* **553** 124213
[28] Kerner B S 2009 *Introduction to modern traffic flow theory and control* (Berlin: Springer) pp. 1–265
[29] Kerner B S and Klenov S L 2002 *J. Phys. A: Math. Gen.* **35** L31
[30] Kerner B S, Klenov S L, Hermanns G and Schreckenberg M 2013 *Physica A* **392** 4083
[31] Zeng J W, Qian Y S, Lv Z W, Yin F, Zhu L P, Zhang Y Z and Xu D J 2021 *Physica A* **574** 125918
[32] Kerner B S, Klenov S L, Hermanns G and Schreckenberg M 2013 *Physica A* **392** 4083
[33] Hu X J, Lin C X, Hao X T, Lu R Y and Liu T H 2021 *Physica A* **584** 126335
[34] Hu X J, Qiao L Q, Hao X T, Lin C X and Liu T H 2022 *Physica A* **605** 127962
[35] Lyu Z L, Hu X J, Zhang F, Liu T H and Cui Z W 2022 *Physica A* **587** 126471
[36] Zhou S R, Ling S, Zhu C Q and Tian J F 2022 *Physica A* **596** 127162
[37] Tian J F, Li G Y, Treiber M, Jiang R, Jia N and Ma S F 2016 *Transp. Res. B Method.* **93** 560
[38] Gao K, Jiang R, Wang B H and Wu Q S 2009 *Physica A* **388** 3233
[39] Kerner B S 2002 *Phys. Rev. E* **65** 046138